

---

# Gaussian Splatting with NeRF-based Color and Opacity

---

Dawid Malarz<sup>\*1</sup> Weronika Smolak<sup>\*1</sup> Jacek Tabor<sup>1</sup> Sławomir Tadeja<sup>2</sup> Przemysław Spurek<sup>1</sup>

## Abstract

*Neural Radiance Fields* (NeRFs) have demonstrated the remarkable potential of neural networks to capture the intricacies of 3D objects. By encoding the shape and color information within neural network weights, NeRFs excel at producing strikingly sharp novel views of 3D objects. Recently, numerous generalizations of NeRFs utilizing generative models have emerged, expanding its versatility. In contrast, *Gaussian Splatting* (GS) offers a similar renders quality with faster training and inference as it does not need neural networks to work. We encode information about the 3D objects in the set of Gaussian distributions that can be rendered in 3D similarly to classical meshes. Unfortunately, GS are difficult to condition since they usually require circa hundred thousand Gaussian components. To mitigate the caveats of both models, we propose a hybrid model that uses GS representation of the 3D object's shape and NeRF-based encoding of color and opacity. Our model uses Gaussian distributions with trainable positions (i.e. means of Gaussian), shape (i.e. covariance of Gaussian), color and opacity, and neural network, which takes parameters of Gaussian and viewing direction to produce changes in color and opacity. Consequently, our model better describes shadows, light reflections, and transparency of 3D objects.

## 1. Introduction

Over recent years, neural rendering has become a significant and, at the same time, prolific area of computer graphics research. The groundbreaking concept of *Neural Radiance Fields* (NeRFs) (Mildenhall et al., 2020) has revolutionized 3D modeling, enabling the creation of complex, high-fidelity 3D scenes from previously unseen angles using only

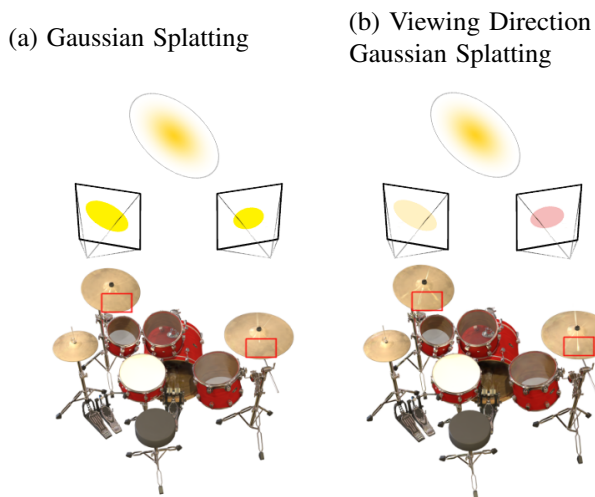


Figure 1. Comparison of Gaussian Splatting (GS) and Viewing Direction Gaussian Splatting (VDGS). In our model, each Gaussian has a different color and opacity, shadows, light reflection, and transparency of 3D objects (see elements in red rectangles).

a minimal set of planar images and corresponding camera positions. This particular neural network architecture harnesses the connection among these images and fundamental methods and techniques of computer graphics, such as ray tracing, to conjure high-quality scenes from previously unseen vantage points.

In NeRFs (Mildenhall et al., 2020), the scene is represented with the help of fully connected, i.e. non-convoluted, network architectures. These networks take as an input a 5D coordinate consisting of camera positions and spatial location. From this data, they are able to generate the color and volume density of each point within the scene. The loss function of NeRF draws inspiration from conventional volume rendering techniques (Kajiya & Von Herzen, 1984), which involve rendering the color of every ray traversing the scene. In essence, NeRF embeds the shape and color information of the object within the neural network's weights.

Various changes can be employed to expedite NeRF training and inference processes. Furthermore, NeRF can be conditioned when used as a component of large generative models, such as diffusion models (Chen et al., 2023) or generative adversarial networks (GANs) (Chan et al., 2022).

<sup>\*</sup>Equal contribution <sup>1</sup>Faculty of Mathematics and Computer Science, Jagiellonian University, Krakow, Poland <sup>2</sup>Department of Engineering, University of Cambridge, Cambridge, UK. Correspondence to: Przemysław Spurek <przemyslaw.spurek@uj.edu.pl>.

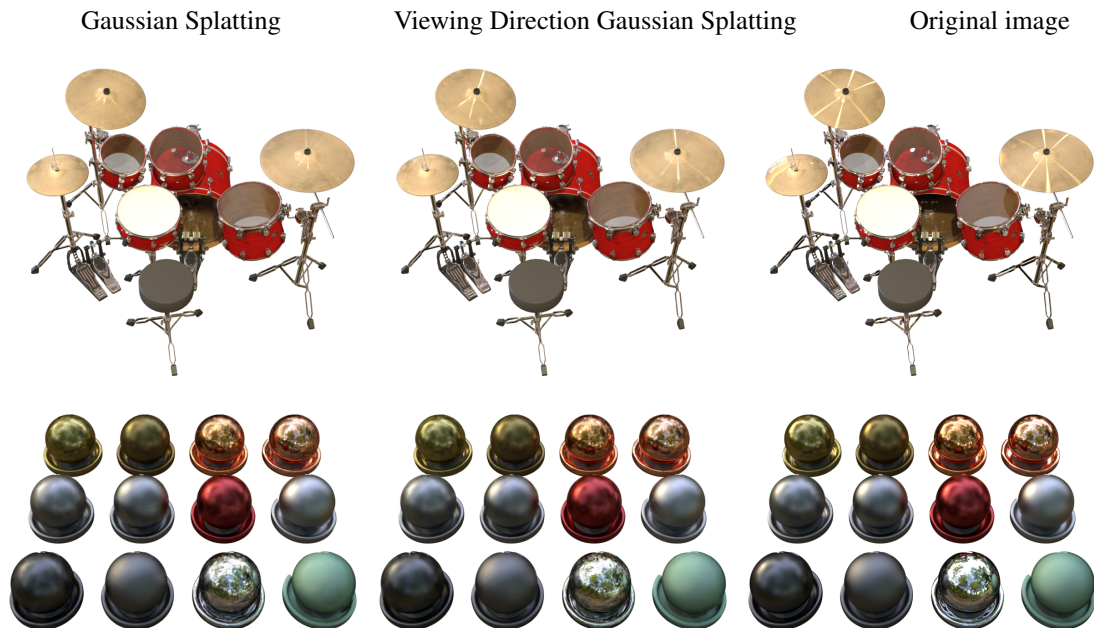


Figure 2. Visual comparison between classical GS and Viewing Direction Gaussian Splatting on the dataset: NeRF Synthetic. As we can see Viewing Direction Gaussian Splatting can better describe shadows, light reflection, and transparency of rendered 3D objects.

NeRF architecture excels at generating crisp renders of new viewpoints in static scenes. However, it faces several limitations, primarily stemming from the time-consuming process of encoding object shapes into neural network weights. In practice, training and inference with NeRF models can take extensive time, making them often impractical for real-time applications.

In comparison, Gaussian Splatting (GS) (Kerbl et al., 2023) provides a similar quality of renders with more rapid in training and inference. This is a consequence of GS not requiring neural networks. We encode information about the 3D objects in a set of Gaussian distributions. These Gaussians can then be used in a similar manner to classical meshes. Consequently, GS can be swiftly developed when needed to, for example, model dynamic scenes (Wu et al., 2023). Unfortunately, GS is hard to condition as it necessitates a hundred thousand Gaussian components.

Both these rendering methods, i.e. NeRFs and SG, offer certain advantages and possess a range of caveats. In this paper, we present Viewing Direction Gaussian Splatting (VDGS)<sup>1</sup>, a new, hybrid approach that uses GS representation of the 3D object’s shape and simultaneously employs NeRF-based encoding of color and opacity. Our model uses Gaussian distributions with trainable positions (i.e., means of Gaussian), shape (i.e., covariance of Gaussian), color, and opacity, as

<sup>1</sup>The source code is available at: <https://github.com/gmum/ViewingDirectionGaussianSplatting>.

well as a neural network, which takes a parameter of Gaussian together with viewing direction to produce changes in the color and opacity.

In summary, the contributions of our work are the following:

- We propose a hybrid architecture utilizing both NeRF and GS and NeRF. We encode the color and opacity using NeRF, whereas GS represents the 3D object’s shape.
- In Viewing Direction Gaussian Splatting color and opacity depend on viewing direction.
- Viewing Direction Gaussian Splatting describe better shadows, light reflection, and transparency in 3D objects.

## 2. Related Works

We can rely on various techniques to represent 3D objects, including voxel grids (Choy et al., 2016), octrees (Häne et al., 2017), multi-view images (Arsalan Soltani et al., 2017), geometry images (Sinha et al., 2016), and finally, point clouds (Yang et al., 2022). An alternative approach is given through *Neural Radiance Field* (NeRF) (Mildenhall et al., 2020).

**NeRF** The aforementioned representations are discrete, which can lead to issues in their applicability in various



Figure 3. Visual comparison between classical GS and Viewing Direction Gaussian Splatting on three distinct datasets, namely, NeRF synthetic (Mildenhall et al., 2020), Tanks and Temples (Knapitsch et al., 2017), and Shiny Blender (Verbin et al., 2022)..

use case scenarios (Spurek et al., 2020). In comparison, NeRF (Mildenhall et al., 2020) utilizes a fully connected architecture to represent a scene. NeRF and its various generalizations (Barron et al., 2021; 2022; Liu et al., 2020; Niemeyer et al., 2022; Roessle et al., 2022; Tancik et al., 2022; Verbin et al., 2022) use differentiable volumetric rendering to generate novel views of a static scene.

The prolonged training time associated with traditional NeRFs has been tackled before with the introduction of Plenoxels (Fridovich-Keil et al., 2022). In this approach we replace the dense voxel representation with a sparse voxel grid, significantly reducing the computational demands. Within this sparse grid, density and spherical harmonics coefficients are stored at each node, enabling the estimation of color based on trilinear interpolation of neighboring voxel values. On the other hand, Sun et al. (2022) delved into optimizing the features of voxel grids to achieve rapid radiance field reconstruction. Müller et al. (2022) refined this approach by partitioning the 3D space into independent multilevel grids to enhance its computational efficiency further. Chen et al. (2022) studies representation 3D object using orthogonal tensor components. A small MLP network then extracts the final color and density from these components using orthogonal projection. Additionally, there are some methods that use supplementary information such as depth maps or point clouds, such as (Azinović et al., 2022; Deng et al., 2022; Roessle et al., 2022). Zimny et al. (2023) proposed a MultiPlane version of NeRF with image-based planes to represent 3D objects. The TriPlane representation from EG3D (Chan et al., 2022) has many applications in the diffusion-based generative model (Chen et al., 2023).

NeRF-based models can render highly sharp renders and be used in large generative models. Unfortunately, NeRF is expensive in training and rendering.

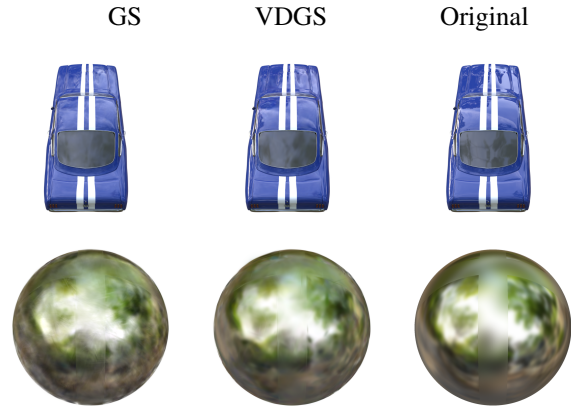


Figure 4. Visual comparison between classical GS and Viewing Direction Gaussian Splatting on the dataset: Shiny Blender.

**Gaussian Splatting** The point-based representations such as Gaussian have been widely used in a variety of fields, including shape reconstruction (Keselman & Hebert, 2023), molecular structures modeling (Blinn, 1982), or the substitution of point-cloud data (Eckart et al., 2016). Moreover, these representations are employed in shadow (Nulkar & Mueller, 2001) and cloud rendering applications (Man, 2006). Recently, 3D Gaussian Splatting (3D-GS) (Kerbl et al., 2023), which combines the concept of point-based rendering and splatting techniques for rendering, has achieved real-time speed with a rendering quality that is comparable to the best MLP-based renderer, Mip-NeRF.

GS offers faster training and inference time than NeRF. Moreover, we do not use a neural network, as all the information is stored in 3D objects. Therefore, such a model finds application in dynamic scene modeling. Moreover, it is easy to combine with a 3D engine dedicated to computer graphics (Kerbl et al., 2023). On the other hand, it is hard



	Mip-NeRF360			Tanks&Temples			Deep Blending		
	SSIM $\uparrow$	PSNR $\uparrow$	LPIPS $\downarrow$	SSIM $\uparrow$	PSNR $\uparrow$	LPIPS $\downarrow$	SSIM $\uparrow$	PSNR $\uparrow$	LPIPS $\downarrow$
Plenoxels	0.626	23.08	0.719	0.379	21.08	0.795	0.510	23.06	0.510
INGP-Base	0.671	25.30	0.371	0.723	21.72	0.330	0.797	23.62	0.423
INGP-Big	0.699	25.59	0.331	0.745	21.92	0.305	0.817	24.96	0.390
M-NeRF360	0.792	27.69	0.237	0.759	22.22	0.257	0.901	29.40	0.245
Gaussian Splatting-7K	0.770	25.60	0.279	0.767	21.20	0.280	0.875	27.78	0.317
Gaussian Splatting-30K	<b>0.815</b>	27.21	<b>0.214</b>	0.841	23.14	0.183	<b>0.903</b>	29.41	0.243
VDGS (Our)	0.809	<b>27.80</b>	0.223	<b>0.845</b>	<b>24.16</b>	<b>0.174</b>	0.900	<b>29.91</b>	<b>0.242</b>

Table 1. Quantitative evaluation of Viewing Direction Gaussian Splatting method compared to previous work, computed over three distinct datasets, namely, NeRF synthetic (Mildenhall et al., 2020), Tanks and Temples (Knapitsch et al., 2017), and Shiny Blender (Verbin et al., 2022).

to condition GS since we have hundreds of thousands of Gaussian components.

In the paper, we present a fiction of NeRF model and GS representation of 3D objects.

### 3. Viewing Direction Gaussian Splatting

Here, we briefly describe the NeRF and GS models to better ground our findings. Next, we provide the details about Viewing Direction Gaussian Splatting the hybrid of the above models.

**NeRF representation of 3D objects** Vanilla NeRF (Mildenhall et al., 2020) is the model for representing complex 3D scenes using neural architectures. NeRF takes a 5D coordinate as input, which includes the spatial location  $\mathbf{x} = (x, y, z)$  and viewing direction  $\mathbf{d} = (\theta, \psi)$  and returns emitted color  $\mathbf{c} = (r, g, b)$  and volume density  $\sigma$ .

A vanilla NeRF employs a collection of images for training. This process entails generating an ensemble of rays that pass through the image and interact with a 3D object represented by a neural network. These interactions, including the observed color and depth, are then used to train the neural network to represent the object’s shape and appearance accurately. NeRF approximates this 3D object with an MLP network:

$$\mathcal{F}_{NeRF}(\mathbf{x}, \mathbf{d}; \Theta) = (\mathbf{c}, \sigma).$$

The MLP parameters,  $\Theta$ , are optimized during training to minimize the discrepancy between the rendered images and the reference images from a given dataset. Consequently, MLP network takes a 3D coordinate as input and outputs a density value along with the radiance (color) in a specified direction.

The loss of NeRF is inspired by classical volume rendering (Kajiya & Von Herzen, 1984). We render the color of all rays passing through the scene. The volume density  $\sigma(\mathbf{x})$  can be interpreted as the differential probability of a ray. The expected color  $C(\mathbf{r})$  of camera ray  $\mathbf{r}(t) = \mathbf{o} + t\mathbf{d}$  (where  $\mathbf{o}$

is ray origin and  $\mathbf{d}$  is direction) can be computed with an integral, but in practice, it is estimated numerically using stratified sampling. The loss is simply the total squared error between the rendered and true pixel colors:

$$\mathcal{L} = \sum_{\mathbf{r} \in R} \|\hat{C}(\mathbf{r}) - C(\mathbf{r})\|_2^2, \quad (1)$$

where  $R$  is the set of rays in each batch, and  $C(\mathbf{r})$ ,  $\hat{C}(\mathbf{r})$  are the ground truth and predicted RGB colors for ray  $\mathbf{r}$ , respectively. The predicted RGB colors  $\hat{C}(\mathbf{r})$  can be obtained using the following equation:

$$\hat{C}(\mathbf{r}) = \sum_{i=1}^N T_i (1 - \exp(-\sigma_i \delta_i)) \mathbf{c}_i, \quad (2)$$

where  $T_i = \exp\left(-\sum_{j=1}^{i-1} \sigma_j \delta_j\right)$  and  $N$  is the number of samples,  $\delta_i$  is the distance between adjacent samples, and  $\sigma_i$  denotes the opacity of sample  $i$ . This function allowing computation of  $\hat{C}(\mathbf{r})$  from the set of  $(\mathbf{c}_i, \sigma_i)$  values is trivially differentiable.

Such approaches to representing 3D objects in neural networks often face limitations due to the neural network’s capacity or the challenging task of precisely locating where camera rays intersect with the scene geometry. Consequently, generating high-resolution images from these representations often necessitates computationally expensive optical ray marching, which can hinder real-time use case scenarios.

**Gaussian Splatting** Gaussian Splatting (GS) model 3D scene by a collection of 3D Gaussians defined by a position (mean), covariance matrix, opacity, and color represented via spherical harmonics (SH) (Fridovich-Keil et al., 2022; Müller et al., 2022).

GS algorithm creates the radiance field representation by a sequence of optimization steps of 3D Gaussian parameters (i.e., position, covariance, opacity, and SH colors). The key



	PSNR $\uparrow$								
	Chair	Drums	Lego	Mic	Materials	Ship	Hotdog	Ficus	Avg.
NeRF	33.00	25.01	32.54	32.91	29.62	28.65	36.18	30.13	31.01
VolSDF	30.57	20.43	29.46	30.53	29.13	25.51	35.11	22.91	27.96
Ref-NeRF	33.98	25.43	35.10	33.65	27.10	29.24	37.04	28.74	31.29
ENVIDR	31.22	22.99	29.55	32.17	29.52	21.57	31.44	26.60	28.13
Gaussian Splatting	35.82	26.17	35.69	35.34	30.00	30.87	37.67	34.83	33.30
GaussianShader	35.83	<b>26.36</b>	<b>35.87</b>	35.23	30.07	30.82	<b>37.85</b>	34.97	33.38
VDGS (Our)	<b>36.13</b>	26.25	35.32	<b>35.74</b>	<b>30.13</b>	<b>31.25</b>	37.55	<b>35.37</b>	<b>33.47</b>
	SSIM $\uparrow$								
NeRF	0.967	0.925	0.961	0.980	0.949	0.856	0.974	0.964	0.947
VolSDF	0.949	0.893	0.951	0.969	0.954	0.842	0.972	0.929	0.932
Ref-NeRF	0.974	0.929	0.975	0.983	0.921	0.864	0.979	0.954	0.947
ENVIDR	0.976	0.930	0.961	0.984	<b>0.968</b>	0.855	0.963	0.987	0.956
Gaussian Splatting	<b>0.987</b>	<b>0.954</b>	<b>0.983</b>	0.991	0.960	<b>0.907</b>	<b>0.985</b>	0.987	<b>0.969</b>
GaussianShader	<b>0.987</b>	0.949	<b>0.983</b>	0.991	0.960	0.905	<b>0.985</b>	0.985	0.968
VDGS (Our)	<b>0.987</b>	0.952	0.980	<b>0.992</b>	0.962	<b>0.907</b>	0.984	<b>0.988</b>	0.969
	LPIPS $\downarrow$								
NeRF	0.046	0.091	0.050	0.028	0.063	0.206	0.121	0.044	0.081
VolSDF	0.056	0.119	0.054	0.191	0.048	0.191	0.043	0.068	0.096
Ref-NeRF	0.029	0.073	0.025	0.018	0.078	0.158	0.028	0.056	0.058
ENVIDR	0.031	0.080	0.054	0.021	0.045	0.228	0.072	<b>0.010</b>	0.067
Gaussian Splatting	<b>0.012</b>	<b>0.037</b>	0.016	<b>0.006</b>	0.034	0.106	0.020	0.012	0.030
GaussianShader	<b>0.012</b>	0.040	<b>0.014</b>	<b>0.006</b>	<b>0.033</b>	<b>0.098</b>	<b>0.019</b>	0.013	<b>0.029</b>
VDGS (Our)	0.013	0.039	0.018	<b>0.006</b>	0.034	0.108	0.022	<b>0.010</b>	0.031

Table 2. The quantitative comparisons (PSNR / SSIM / LPIPS) on NeRF Synthetic dataset.

to the efficiency of GS is the rendering process, which uses projections of Gaussian components.

In GS, we use a dense set of 3D Gaussians

$$\mathcal{G} = \{(\mathcal{N}(m_i, \Sigma_i), \sigma_i, c_i)\}_{i=1}^n,$$

where  $m_i$  is position,  $\Sigma_i$  is covariance,  $\sigma_i$  is opacity, and  $c$  is SH colors of  $i$ -th component.

GS optimization is based on a cycle of rendering and comparing the generated image to the training views in the collected data. Unfortunately, 3D to 2D projection can lead to incorrect geometry placement. Therefore, GS optimization must be able to create, destroy, and move geometry if it is incorrectly positioned. The quality of the parameters of the 3D Gaussian covariances is essential for the representation’s compactness, as large homogeneous areas can be captured with a small number of large anisotropic Gaussians.

GS starts with a limited number of points and then employs a strategy that involves creating new components and eliminating unnecessary ones. Every hundred iterations, GS eliminates any Gaussians with an opacity lower than a specific limit. At the same time, new Gaussians are generated in unoccupied areas of 3D space to fill vacant areas. The optimization process in GS is complicated, but it can be trained very effectively thanks to robust implementation and the usage of CUDA kernels.

### Viewing Direction Gaussian Splatting

**Viewing Direction Gaussian Splatting** In our approach, we use GS to model 3D shapes, while a NeRF-based neural network produces colors and opacity. Our model consists of the Gaussian Splatting representation:

$$\mathcal{G} = \{(\mathcal{N}(m_i, \Sigma_i), \sigma_i, c_i)\}_{i=1}^n,$$

and the MLP network:

$$\mathcal{F}_{VDGS}(m, \Sigma, c, \mathbf{d}; \Theta) = \Delta\sigma(\mathbf{d}),$$

which takes parameters of Gaussian distribution and viewing direction  $\mathbf{d}$  to returns emitted color update  $\Delta\mathbf{c}(\mathbf{d})$  and volume density update  $\Delta\sigma(\mathbf{d})$ . The model is parameterized by  $\Theta$  and trained to change color and opacity depending on viewing direction.

The final Viewing Direction Gaussian Splatting model is given by:

$$(\mathcal{G}, \mathcal{F}_{VDGS}) = \{(\mathcal{N}(m_i, \Sigma_i), \sigma_i \cdot \Delta\sigma_i(\mathbf{d}), \mathbf{c}_i)\}_{i=1}^n,$$

where

$$\Delta\sigma_i(\mathbf{d}) = \mathcal{F}_{VDGS}(m_i, \Sigma_i, c_i, \mathbf{d}).$$

In practice, we have two components: GS and NeRF. GS is used to produce the shape and color of the objects. All Gaussian components have color and transparent, which do not depend on viewing direction. Thanks to GS, we model the universal colors of 3D objects. Depending on the camera position, the NeRF component can add minor color changes

	PSNR $\uparrow$						
	Car	Ball	Helmet	Teapot	Toaster	Coffee	Avg.
NVDiffRec (Munkberg et al., 2022)	27.98	21.77	26.97	40.44	24.31	30.74	28.70
NVDiffMC (Hasselgren et al., 2022)	25.93	30.85	26.27	38.44	22.18	29.60	28.88
Ref-NeRF (Verbin et al., 2022)	<b>30.41</b>	29.14	29.92	45.19	25.29	<b>33.99</b>	32.32
NeRO (Liu et al., 2023)	25.53	30.26	29.20	38.70	26.46	28.89	29.84
ENVIDR (Liang et al., 2023)	28.46	<b>38.89</b>	<b>32.73</b>	41.59	26.11	29.48	<b>32.88</b>
Guassian Splatting (Kerbl et al., 2023)	27.24	27.69	28.32	45.68	20.99	32.32	30.37
GaussianShader (Jiang et al., 2023)	27.90	30.98	28.32	<b>45.86</b>	<b>26.21</b>	32.39	31.94
VDGS (Our)	26.99	27.87	28.18	45.39	21.53	32.16	30.35
SSIM $\uparrow$							
NVDiffRec (Munkberg et al., 2022)	0.963	0.858	0.951	<b>0.996</b>	0.928	0.973	0.945
NVDiffMC (Hasselgren et al., 2022)	0.940	0.940	0.940	0.995	0.886	0.965	0.944
Ref-NeRF (Verbin et al., 2022)	0.949	0.956	0.955	0.995	0.910	<b>0.972</b>	0.956
NeRO (Liu et al., 2023)	0.949	0.974	0.971	0.995	0.929	0.956	0.962
ENVIDR (Liang et al., 2023)	<b>0.961</b>	<b>0.991</b>	<b>0.980</b>	<b>0.996</b>	<b>0.939</b>	0.949	<b>0.969</b>
Guassian Splatting (Kerbl et al., 2023)	0.930	0.937	0.951	<b>0.996</b>	0.895	0.971	0.947
GaussianShader (Jiang et al., 2023)	0.931	0.965	0.950	<b>0.996</b>	0.929	0.971	0.957
VDGS (Our)	0.938	0.944	0.949	<b>0.996</b>	0.899	0.971	0.949
LPIPS $\downarrow$							
NVDiffRec (Munkberg et al., 2022)	0.045	0.297	0.118	0.011	0.169	0.076	0.119
NVDiffMC (Hasselgren et al., 2022)	0.077	0.312	0.157	0.014	0.225	0.097	0.147
Ref-NeRF (Verbin et al., 2022)	0.051	0.307	0.087	0.013	0.118	0.082	0.109
NeRO (Liu et al., 2023)	0.074	0.094	<b>0.050</b>	0.012	0.089	0.110	0.072
ENVIDR (Liang et al., 2023)	0.049	<b>0.067</b>	0.051	0.011	0.116	0.139	0.072
Guassian Splatting (Kerbl et al., 2023)	0.047	0.161	0.079	<b>0.007</b>	0.126	<b>0.078</b>	0.083
GaussianShader (Jiang et al., 2023)	<b>0.045</b>	0.121	<b>0.076</b>	<b>0.007</b>	<b>0.079</b>	<b>0.078</b>	<b>0.068</b>
VDGS (Our)	0.049	0.143	0.073	<b>0.007</b>	0.101	0.079	0.075

Table 3. The quantitative comparisons (PSNR / SSIM / LPIPS) on Shiny Blender dataset (Verbin et al., 2022).

and transparency to the objects. Our model can add viewing direction-based changes. Therefore, it allows the modeling of light reflection and transparency of the objects.

## 4. Experiments

**Datasets** To comprehensively validate the effectiveness of VDGS, we conducted an evaluation on various datasets: a) widely-used NVS dataset, i.e., the *NeRF Synthetic* (Mildenhall et al., 2020), b) real-world, large-scale scenes dataset, i.e., the *Tanks and Temples* (Knapitsch et al., 2017), and c) reflective objects datasets, i.e., the *Shiny Blender* (Verbin et al., 2022).

**Dataset: Tanks and Temples** We also evaluated our model on larger-scale environments by comparing our solution on the Tanks and Temples dataset (Knapitsch et al., 2017). Tab. 1 and visual comparisons in Fig. 3 shows that we are able to better model light reflexes and shadows than either GS and NeRF.

**Dataset: NeRF Synthetic** We first evaluate our model on the NeRF Synthetic dataset (Mildenhall et al., 2020), which contains objects with complex geometry and realistic non-Lambertian materials. We show the quantitative results in Tab. 2 and visual comparisons in Fig. 2. The results show that our approach achieves better results than both Gaussian

Splatting and neural rendering methods.

**Dataset: Shiny Blender** Viewing Direction Gaussian Splatting can plausible model shadows, light reflection, and transparency in 3D objects. Therefore, we decided to evaluate our hybrid approach on the Shiny Blender dataset (Verbin et al., 2022). Once again, visual comparisons in Fig. 4 and quantitative results in Tab. 3 show that we obtain comparable results to NeRF and GS approaches but slightly worse than dedicated method GaussianShader (Jiang et al., 2023).

## 5. Conclusions

This paper presents a new neural rendering strategy that leverages two main concepts, NeRF and GS. We represent a 3D scene with a set of Gaussian components and a neural network that can change the color and opacity of Gaussians concerning viewing direction. This approach inherited the best elements from the NeRF and GS methods. We have quick training and inference time and we are able to model shadows, light reflections, and transparency of 3D objects.

The experimental section shows that Viewing Direction Gaussian Splatting gives better results than NeRF as well as the Gaussian Splatting model.

---

## References

- Arsalan Soltani, A., Huang, H., Wu, J., Kulkarni, T. D., and Tenenbaum, J. B. Synthesizing 3d shapes via modeling multi-view depth maps and silhouettes with deep generative networks. In *Proceedings of the IEEE conference on computer vision and pattern recognition*, pp. 1511–1519, 2017.
- Azinović, D., Martin-Brualla, R., Goldman, D. B., Nießner, M., and Thies, J. Neural rgb-d surface reconstruction. In *Proceedings of the IEEE/CVF Conference on Computer Vision and Pattern Recognition*, pp. 6290–6301, 2022.
- Barron, J. T., Mildenhall, B., Tancik, M., Hedman, P., Martin-Brualla, R., and Srinivasan, P. P. Mip-nerf: A multiscale representation for anti-aliasing neural radiance fields. In *Proceedings of the IEEE/CVF International Conference on Computer Vision*, pp. 5855–5864, 2021.
- Barron, J. T., Mildenhall, B., Verbin, D., Srinivasan, P. P., and Hedman, P. Mip-nerf 360: Unbounded anti-aliased neural radiance fields. In *Proceedings of the IEEE/CVF Conference on Computer Vision and Pattern Recognition*, pp. 5470–5479, 2022.
- Blinn, J. F. A generalization of algebraic surface drawing. *ACM transactions on graphics (TOG)*, 1(3):235–256, 1982.
- Chan, E. R., Lin, C. Z., Chan, M. A., Nagano, K., Pan, B., De Mello, S., Gallo, O., Guibas, L. J., Tremblay, J., Khamis, S., et al. Efficient geometry-aware 3d generative adversarial networks. In *Proceedings of the IEEE/CVF Conference on Computer Vision and Pattern Recognition*, pp. 16123–16133, 2022.
- Chen, A., Xu, Z., Geiger, A., Yu, J., and Su, H. Tensorf: Tensorial radiance fields. In *Computer Vision—ECCV 2022: 17th European Conference, Tel Aviv, Israel, October 23–27, 2022, Proceedings, Part XXXII*, pp. 333–350. Springer, 2022.
- Chen, H., Gu, J., Chen, A., Tian, W., Tu, Z., Liu, L., and Su, H. Single-stage diffusion nerf: A unified approach to 3d generation and reconstruction. In *ICCV*, 2023.
- Choy, C. B., Xu, D., Gwak, J., Chen, K., and Savarese, S. 3d-r2n2: A unified approach for single and multi-view 3d object reconstruction. In *European conference on computer vision*, pp. 628–644. Springer, 2016.
- Deng, K., Liu, A., Zhu, J.-Y., and Ramanan, D. Depth-supervised nerf: Fewer views and faster training for free. In *Proceedings of the IEEE/CVF Conference on Computer Vision and Pattern Recognition*, pp. 12882–12891, 2022.
- Eckart, B., Kim, K., Troccoli, A., Kelly, A., and Kautz, J. Accelerated generative models for 3d point cloud data. In *Proceedings of the IEEE conference on computer vision and pattern recognition*, pp. 5497–5505, 2016.
- Fridovich-Keil, S., Yu, A., Tancik, M., Chen, Q., Recht, B., and Kanazawa, A. Plenoxels: Radiance fields without neural networks. In *CVPR*, pp. 5501–5510, 2022.
- Häne, C., Tulsiani, S., and Malik, J. Hierarchical surface prediction for 3d object reconstruction. In *2017 International Conference on 3D Vision (3DV)*, pp. 412–420. IEEE, 2017.
- Hasselgren, J., Hofmann, N., and Munkberg, J. Shape, light, and material decomposition from images using monte carlo rendering and denoising. *Advances in Neural Information Processing Systems*, 35:22856–22869, 2022.
- Jiang, Y., Tu, J., Liu, Y., Gao, X., Long, X., Wang, W., and Ma, Y. Gaussianshader: 3d gaussian splatting with shading functions for reflective surfaces. *arXiv preprint arXiv:2311.17977*, 2023.
- Kajiya, J. T. and Von Herzen, B. P. Ray tracing volume densities. *ACM SIGGRAPH computer graphics*, 18(3): 165–174, 1984.
- Kerbl, B., Kopanas, G., Leimkühler, T., and Drettakis, G. 3d gaussian splatting for real-time radiance field rendering. *ACM Transactions on Graphics*, 42(4), 2023.
- Keselman, L. and Hebert, M. Flexible techniques for differentiable rendering with 3d gaussians. *arXiv preprint arXiv:2308.14737*, 2023.
- Knapitsch, A., Park, J., Zhou, Q.-Y., and Koltun, V. Tanks and temples: Benchmarking large-scale scene reconstruction. *ACM Transactions on Graphics (ToG)*, 36(4):1–13, 2017.
- Liang, R., Chen, H., Li, C., Chen, F., Panneer, S., and Vijaykumar, N. Envidr: Implicit differentiable renderer with neural environment lighting. *arXiv preprint arXiv:2303.13022*, 2023.
- Liu, L., Gu, J., Zaw Lin, K., Chua, T.-S., and Theobalt, C. Neural sparse voxel fields. *Advances in Neural Information Processing Systems*, 33:15651–15663, 2020.
- Liu, Y., Wang, P., Lin, C., Long, X., Wang, J., Liu, L., Komura, T., and Wang, W. Nero: Neural geometry and brdf reconstruction of reflective objects from multiview images. *arXiv preprint arXiv:2305.17398*, 2023.
- Man, P. Generating and real-time rendering of clouds. In *Central European seminar on computer graphics*, volume 1. Citeseer Castá-Papiernicka, Slovakia, 2006.



- 
- Mildenhall, B., Srinivasan, P. P., Tancik, M., Barron, J. T., Ramamoorthi, R., and Ng, R. Nerf: Representing scenes as neural radiance fields for view synthesis. In *ECCV*, 2020.
- Müller, T., Evans, A., Schied, C., and Keller, A. Instant neural graphics primitives with a multiresolution hash encoding. *ACM Transactions on Graphics (ToG)*, 41(4): 1–15, 2022.
- Munkberg, J., Hasselgren, J., Shen, T., Gao, J., Chen, W., Evans, A., Müller, T., and Fidler, S. Extracting triangular 3d models, materials, and lighting from images. In *Proceedings of the IEEE/CVF Conference on Computer Vision and Pattern Recognition*, pp. 8280–8290, 2022.
- Niemeyer, M., Barron, J. T., Mildenhall, B., Sajjadi, M. S., Geiger, A., and Radwan, N. Regnerf: Regularizing neural radiance fields for view synthesis from sparse inputs. In *Proceedings of the IEEE/CVF Conference on Computer Vision and Pattern Recognition*, pp. 5480–5490, 2022.
- Nulkar, M. and Mueller, K. Splatting with shadows. In *Volume Graphics 2001: Proceedings of the Joint IEEE TCVG and Eurographics Workshop in Stony Brook, New York, USA, June 21–22, 2001*, pp. 35–49. Springer, 2001.
- Roessle, B., Barron, J. T., Mildenhall, B., Srinivasan, P. P., and Nießner, M. Dense depth priors for neural radiance fields from sparse input views. In *Proceedings of the IEEE/CVF Conference on Computer Vision and Pattern Recognition*, pp. 12892–12901, 2022.
- Sinha, A., Bai, J., and Ramani, K. Deep learning 3d shape surfaces using geometry images. In *European Conference on Computer Vision*, pp. 223–240. Springer, 2016.
- Spurek, P., Winczowski, S., Tabor, J., Zamorski, M., Zieba, M., and Trzciński, T. Hypernetwork approach to generating point clouds. *Proceedings of Machine Learning Research*, 119, 2020.
- Sun, C., Sun, M., and Chen, H.-T. Direct voxel grid optimization: Super-fast convergence for radiance fields reconstruction. In *CVPR*, pp. 5459–5469, 2022.
- Tancik, M., Casser, V., Yan, X., Pradhan, S., Mildenhall, B., Srinivasan, P. P., Barron, J. T., and Kretzschmar, H. Block-nerf: Scalable large scene neural view synthesis. In *Proceedings of the IEEE/CVF Conference on Computer Vision and Pattern Recognition*, pp. 8248–8258, 2022.
- Verbin, D., Hedman, P., Mildenhall, B., Zickler, T., Barron, J. T., and Srinivasan, P. P. Ref-nerf: Structured view-dependent appearance for neural radiance fields. In *2022 IEEE/CVF Conference on Computer Vision and Pattern Recognition (CVPR)*, pp. 5481–5490. IEEE, 2022.
- Wu, G., Yi, T., Fang, J., Xie, L., Zhang, X., Wei, W., Liu, W., Tian, Q., and Wang, X. 4d gaussian splatting for real-time dynamic scene rendering. *arXiv preprint arXiv:2310.08528*, 2023.
- Yang, F., Davoine, F., Wang, H., and Jin, Z. Continuous conditional random field convolution for point cloud segmentation. *Pattern Recognition*, 122:108357, 2022.
- Zimny, D., Tabor, J., Zięba, M., and Spurek, P. Multiplanerf: Neural radiance field with non-trainable representation. *arXiv preprint arXiv:2305.10579*, 2023.